



Detailed numerical simulations of the autoignition of single *n*-heptane droplets in air

R. Stauch*, S. Lipp, U. Maas

Institut für Technische Thermodynamik, Universität Karlsruhe, Kaiserstrasse 12, D-76128 Karlsruhe, Germany

Received 20 April 2005; received in revised form 7 December 2005; accepted 20 December 2005

Available online 3 February 2006

Abstract

The autoignition process of single *n*-heptane droplets in air is simulated for spherical symmetry and at constant pressure. Using a detailed transport model and detailed chemical kinetics, the governing equations of the two phases are solved in a fully coupled way. The ambient gas temperature is varied from 600 to 2000 K. Simulations are performed for isobaric conditions. The initial droplet radius ranges from 10 to 200 μm . The influence of different physical parameters, such as ambient pressure, droplet radius, or initial conditions, on the ignition delay time and the location of the ignition is investigated. The gas temperature turns out to be the parameter dominating the ignition process. The droplet temperature shows a minor influence on the ignition delay time. The influence of the droplet radius on the ignition delay shows a high sensitivity to other ambient conditions, such as ambient temperature and pressure.

© 2006 The Combustion Institute. Published by Elsevier Inc. All rights reserved.

Keywords: Droplet; Detailed simulation; Ignition; *n*-Heptane

1. Introduction

A detailed understanding of droplet ignition and combustion is of interest with a view to a reliable description and prediction of spray combustion, which is important in many technical applications, such as LPP gas turbines [1] or combustion engines [2]. Especially, a detailed understanding of the basic physical and chemical processes, such as vaporization, transport and chemical kinetics, is required for a reliable modeling. The status of spray combustion modeling has been reviewed, for instance, by Law [3], Faeth [4], and Chiu [5]. Flamelet modeling of turbu-

lent spray flames based on flame libraries has been performed by Hollmann and Gutheil [6]. A crucial issue in simulating spray combustion is the modeling of the vaporization of the droplets. Widely used modeling assumptions, such as the d^2 -law [7–9] and the 1/3-rule [9–11], have to be validated by detailed simulations of the underlying physical and chemical processes. Moreover, the modeling of spray combustion, including ignition phenomena, is an emerging research area [12]. The autoignition of fuel droplets is governed by the complex interaction of droplet heating, vaporization, and chemical kinetics. Because of this complex interaction, a detailed description of the chemical and physical processes is required. The chemical kinetics of higher hydrocarbons in the gas phase is characterized by a large number of chemical species and elementary reactions. Hence, due to the high computational effort, regimes are investi-

* Corresponding author.

E-mail address: stauch@itt.mach.uni-karlsruhe.de

(R. Stauch).

gated that can be reduced to one- or two-dimensional geometries. The simplest model of the fuel spray ignition process is the ignition of a single fuel droplet. Assuming microgravity conditions, i.e., no gravitation and no relative motion of droplet and gas phase, the system can be regarded as one-dimensional.

Many experimental investigations focus on the combustion of single fuel droplets under microgravity conditions [13–21]. Detailed investigations including numerical simulations, allowing detailed insight into the combustion process, have been reported for the fuels methanol [22–25], ethanol [26], and *n*-heptane [27–30] in air. Only a few studies focus on the ignition of fuel droplets of higher hydrocarbons [30–37]. Takei et al. [31], Nakanishi et al. [33], and Tanabe et al. [34] have determined ignition delay times of droplets experimentally. Tsukamoto et al. account for chemical kinetics by a one-step irreversible overall reaction [32]. Schnaubelt et al. investigate the ignition process of *n*-heptane and *n*-decane [35,36] experimentally and numerically. Moriue et al. simulate the ignition of a fuel droplet in a closed volume [37]. However, the influence of the ambient gas temperature and the ambient pressure on the ignition process in the case of autoignition has not been investigated extensively for the ignition of higher hydrocarbons (based on detailed numerical simulations). To our knowledge, the only ignition delay times, which have been determined numerically, are restricted to ambient gas temperatures below 1100 K [30,33,35–37]. The dependence of the ignition delay time on ambient pressure is studied numerically by Tsukamoto et al. [32] for an ambient gas temperature of 850 K and experimentally by Nakanishi et al. [33]. With regard to technical applications, the influence of these ambient parameters is of major interest. With higher ambient temperatures and a wider pressure range, all possible conditions for igniting and burning droplets can be covered. So it is possible to generate libraries, which can be used for flamelet modeling of spray combustion [6]. Among others, the ignition of droplets in a dilute spray provoked by a hot environment (e.g., caused by other already burning droplets) can be described. Furthermore, with a wider ambient temperature and pressure range the various ignition–combustion scenarios and the multistate behavior of burning droplets can be described more precisely [5,12].

In this study a detailed numerical simulation model for the ignition and combustion of single fuel droplets is presented. The performed simulations allow a detailed insight into the physical and chemical processes of the autoignition. Spherical symmetry is assumed, which allows one-dimensional description of the problem. Results of numerical simulations of the ignition and combustion of single *n*-heptane

droplets in an isobaric environment are presented. The influence of the ambient gas temperature and the ambient pressure on the ignition process is investigated in the range from 600 to 2000 K and 1 to 40 bar. The droplet radius varies from 10 to 200 μm , which is of interest for the description of technical sprays. The numerical simulations are performed using the fuel *n*-heptane to ensure affinity to technical fuels, such as gasoline.

2. Mathematical model

2.1. Governing equations

The presented model describes a single fuel droplet surrounded by an ambient gas phase with spherical symmetry and constant pressure. This makes it possible to formulate the system of governing equations in terms of the radial coordinate and time. The resulting one-dimensional conservation equations can be found in [38]. To overcome difficulties with the discretization of the convective terms, the equation system in the gas phase is transformed into modified Lagrangian coordinates,

$$f(r, t) \rightarrow f(\psi, t), \quad (1)$$

$$\psi(r, t) = \int_{r_D}^r \rho(r, t) r^2 dr, \quad (2)$$

where r denotes the spatial coordinate, r_D the radius of the surface of the droplet, t the time, ρ the density, and ψ the Lagrangian-like coordinate, and the transformation is given by

$$\left(\frac{\partial r}{\partial t}\right)_\psi = v - \frac{z}{\rho r^2}, \quad (3)$$

$$\left(\frac{\partial}{\partial r}\right)_t = \rho r^2 \left(\frac{\partial}{\partial \psi}\right)_t, \quad (4)$$

$$\left(\frac{\partial}{\partial t}\right)_r = \left(\frac{\partial}{\partial t}\right)_\psi - \rho v r^2 \left(\frac{\partial}{\partial \psi}\right)_t + z \left(\frac{\partial}{\partial \psi}\right)_t. \quad (5)$$

In this way, the continuity equation is implicitly fulfilled. Instead of the continuity equation, the transformation equation has to be solved. The term $z/\rho r^2$ in (3) makes it possible to fix the coordinate system to the droplet surface (in contrast to standard Lagrangian coordinates, where the Lagrangian coordinate is fixed to a volume element). The value of z is obtained from the condition

$$0 = \left(\frac{\partial r}{\partial t}\right)_\psi \Big|_{\psi=\psi_0} = v(\psi_0) - \frac{z}{\rho(\psi_0)r_D^2}, \quad (6)$$

where ψ_0 denotes the origin of the coordinate system, which is located at r_D . After the transformation the

governing equations in the gas phase read

$$\left(\frac{\partial r}{\partial \psi}\right)_t = \frac{1}{\rho r^2}, \quad (7)$$

$$\frac{\partial w_i}{\partial t} + z \frac{\partial w_i}{\partial \psi} + \frac{\partial}{\partial \psi}(r^2 j_i) = \frac{\dot{\omega}_i M_i}{\rho}, \quad (8)$$

$$\begin{aligned} \frac{\partial T}{\partial t} - \frac{1}{\rho C_p} \frac{\partial p}{\partial t} + z \frac{\partial T}{\partial \psi} - \frac{1}{C_p} \frac{\partial}{\partial \psi} \left(\rho r^4 \lambda \frac{\partial T}{\partial \psi} \right) \\ - \frac{r^2}{C_p} \sum_{i=1}^{n_S} j_i C_{pi} \frac{\partial T}{\partial \psi} + \frac{1}{\rho C_p} \sum_{i=1}^{n_S} \dot{\omega}_i h_i M_i = 0, \end{aligned} \quad (9)$$

$$\rho = \frac{p \bar{M}}{RT}, \quad (10)$$

where w_i is the mass fraction, j_i the diffusion flux, $\dot{\omega}_i$ the molar rate of formation, and M_i the molar mass of species i , p the pressure, T the temperature, C_p the molar heat capacity at constant pressure, λ the heat conductivity, and C_{pi} and h_i the molar heat capacity and the specific enthalpy of species i .

Uniform pressure is assumed, and therefore the momentum conservation equation is replaced by $(\partial p / \partial \psi)_t = 0$ (low-Mach-number approximation; see, e.g., [38]). Note that a transformation into modified Lagrangian coordinates is necessary to allow this replacement of the momentum equation.

Analogous to the gas phase, the equation system of the liquid phase is transformed into Lagrangian coordinates (a modification due to an inflowing mass is not necessary in this case):

$$\psi_D^0(t) = \int_0^{r_D(t)} \rho r^2 dr. \quad (11)$$

$\psi_D^0(t)$ is proportional to the mass of the droplet $m_D(t)$, which depends on time:

$$\psi_D^0(t) = \frac{m_D(t)}{4\pi}. \quad (12)$$

Because of the mass loss of the droplet, $\psi_D^0(t)$ decreases with time. Therefore a further transformation is performed to fix the coordinate system to the droplet surface:

$$f(r, t) \rightarrow f(\psi, t) \rightarrow f(\eta, t), \quad (13)$$

$$\eta = \frac{\psi}{\psi_D^0(t)}. \quad (14)$$

The transformation of the differential operators is then given by

$$\left(\frac{\partial}{\partial \psi}\right)_t = \frac{1}{\psi_D^0} \left(\frac{\partial}{\partial \eta}\right)_t, \quad (15)$$

$$\left(\frac{\partial}{\partial t}\right)_\psi = \left(\frac{\partial}{\partial t}\right)_\eta - \frac{1}{\psi_D^0} (\eta \vartheta^0) \left(\frac{\partial}{\partial \eta}\right)_t, \quad (16)$$

with

$$\vartheta^0(t) = \frac{d\psi_D^0}{dt} = -(\phi_{\text{vap}} - \sum R_i) \cdot r_D^2, \quad (17)$$

where ϕ_{vap} denotes the vaporization rate, R_i the surface reaction rate of species i , and r_D the droplet radius. Thus, the governing equations in the liquid phase read

$$\left(\frac{\partial r}{\partial \eta}\right)_t = \frac{\psi_D^0}{\rho r^2}, \quad (18)$$

$$\frac{\partial w_i}{\partial t} - \frac{1}{\psi_D^0} (\eta \vartheta^0) \frac{\partial w_i}{\partial \eta} + \frac{1}{\psi_D^0} \frac{\partial}{\partial \eta} (r^2 j_i) = 0, \quad (19)$$

$$\begin{aligned} \frac{\partial T}{\partial t} - \frac{1}{\psi_D^0} (\eta \vartheta^0) \frac{\partial T}{\partial \eta} - \frac{1}{C_p \psi_D^0} \frac{\partial}{\partial \eta} \left(\rho r^4 \lambda \frac{1}{\psi_D^0} \frac{\partial T}{\partial \eta} \right) \\ - \frac{r^2}{C_p} \sum_{i=1}^{n_S} j_i C_{pi} \frac{1}{\psi_D^0} \frac{\partial T}{\partial \eta} = 0, \end{aligned} \quad (20)$$

$$\rho = \rho(w_1, \dots, w_{n_S}, p, T). \quad (21)$$

The equations describe the case of multicomponent droplets consisting of more than one liquid species ($n_S > 1$). In the presented case of *n*-heptane droplets, only one liquid species is present, and the species conservation equation has not to be solved in the droplet.

2.2. Boundary conditions

Boundary conditions have to be specified in the center of the droplet, at the interface, and at the outer boundary. In the center of the droplet, standard symmetry boundary conditions are applied. At the outer boundary, far away from the droplet surface, Dirichlet boundary conditions are assumed for the temperature and the species concentrations.

At the interface, boundary conditions describe the local phase transition. The temperature profile is continuous across the interface:

$$T_g = T_l \quad \text{at } r = r_D. \quad (22)$$

A vaporization model accounts for the coupling of the liquid phase and the gas phase during the simulation process. A local phase equilibrium was modeled by interface equations:

$$\phi_{\text{vap}} = \frac{-\sum_{j\text{vap}} j_j^g - \sum_{j\text{vap}} w_j \sum_i R_i^g + \sum_{j\text{vap}} R_j^g}{\sum_{j\text{vap}} p_j M_j / p \bar{M} - 1}, \quad (23)$$

$$0 = \rho \cdot v_n - \phi_{\text{vap}} - \sum_i R_i^g, \quad (24)$$

$$0 = \phi_{\text{vap}}(w_i - \epsilon_i) + j_i + w_i \sum_j R_j^g - R_i^g, \quad (25)$$

$$0 = \sum_i \epsilon_i \cdot \phi_{\text{vap}} \cdot \Delta h_{\text{vap},i} + j_{\text{q}}^{\text{g}} - j_{\text{q}}^{\text{l}} + \sum_i R_i^{\text{g}} \bar{h}_i^{\text{g}} + \sum_i R_i^{\text{l}} \bar{h}_i^{\text{l}} \quad (26)$$

The index g denotes the gas phase, the index l the liquid phase. ϕ_{vap} denotes the vaporization rate, w_i the mass fraction of species i , R_i the surface reaction rate of species i , j_{vap} the index of the vaporizing species, p_j the partial pressure of species j , p the pressure, M_j the molar mass of species j , \bar{M} the mean molar mass, ρ the density, v_n the normal velocity, $\epsilon_i = \dot{m}_i / \dot{m}$ the fraction of vaporizing mass, j_i the diffusion flux density of species i (gas phase), $\Delta h_{\text{vap},i}$ the enthalpy of vaporization of species i , and j_{q} the heat flux density.

The modeling of the phase transition, i.e., the interface equations, and the boundary conditions are in accordance with the work of Cho et al. [22,23] and Jackson and Avedisian [27] (note, however, that the numerical method differs from their approach). The modeling differs from the model of Stapf [24], where the vaporization rate is calculated differently.

In the presented case of a liquid n -heptane droplet, surface reactions are not taken into account ($R_i = 0$). Furthermore, $\epsilon = 1$, because only single-component fuels are simulated.

2.3. Reaction mechanism and transport model

The chemical kinetics is modeled by the detailed n -heptane reaction mechanism of Golovitchev [39], including 62 chemical species and 572 elementary reactions. The mechanism is valid for low-temperature as well as high-temperature kinetics. The transport processes are also modeled in detail. The Dufour effect and diffusion by pressure gradients are neglected, because they are negligible compared to the mass diffusion. Fourier's law is used to determine the heat fluxes. For the determination of the diffusion coefficients the approximation of Hirschfelder and Curtiss [40] is used. The liquid-phase properties are calculated based on data correlations taken from Reid et al. [41]. The approximation of Latini et al. is used to calculate the heat conductivities, the approximation of Rowlinson and Bondi to calculate the specific heat capacities. The necessary properties to model the phase transition are also taken from Reid et al. [41]. The vapor pressure is calculated using the Wagner equation; the enthalpy of vaporization is calculated by the approximation of Riedel and Watson.

2.4. Numerical solution

The simulated domain enfolds 100 droplet diameters. It is discretized by the method of lines using

finite differences. The governing equations in the gas phase are spatially discretized by central differences on a nonequidistant grid. Because of the different length scales of nonstationary combustion processes, a regridding procedure based on a grid function is implemented [38,42]. This regridding procedure guarantees a sufficiently high number of grid points in regions where steep gradients appear, e.g., at the flame zone or close to the droplet surface. The interpolation of the governing variables onto the new grid points is based on piecewise monotonic cubic Hermite interpolation [43]. In the liquid phase the equation system is also discretized on a nonequidistant grid. The mesh is refined toward the center of the droplet due to the symmetry boundary conditions and toward the droplet surface, where the steepest gradients in the liquid phase appear. The resulting large and stiff system of ordinary differential and algebraic equations is solved by the linearly implicit extrapolation method LIMEX [44].

3. Results and discussion

The model presented above has been used to simulate the autoignition and combustion of single n -heptane droplets in air. Simulations are performed for isobaric conditions with ambient pressure $p = 7$ bar, which is comparable to the conditions in gas turbines. The droplet radius varies from 10 to 200 μm , which is a significant range for technical sprays.

3.1. Vaporization rates

The temporal evolution of the droplet diameter is plotted in Fig. 1 for ambient gas temperatures of $T_{\text{G}} = 1200$ and 1600 K and an ambient pressure of $p = 1$ bar. This pressure is chosen to allow comparison of the vaporization rate with values taken from literature. To characterize the vaporization process after the ignition of the droplet, the temporal evolution of the droplet diameter was analyzed. After ignition

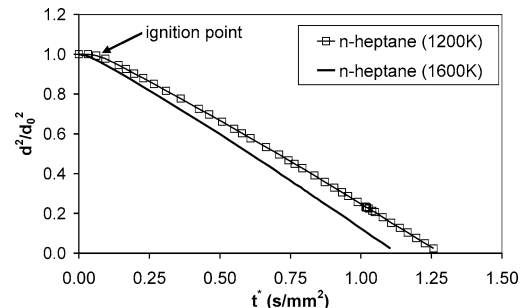


Fig. 1. Temporal evolution of the normalized diameter of an n -heptane droplet in air ($p = 1$ bar, $r_{\text{D}} = 200 \mu\text{m}$).

the droplet diameter follows the d^2 -law

$$d^2 = d_0^2 - K \cdot t \quad (27)$$

in all studied cases. Due to (27) both axes in Fig. 1 are scaled by the square of the initial droplet diameter to simplify the determination of the vaporization rate K . However, as one can see in Fig. 1, the droplet diameter does not follow the d^2 -law right from the beginning of the simulation. There exists an initial phase before ignition due to droplet heating, where the droplet diameter remains almost constant or even increases [45]. Moreover, the vaporization rate of a fuel droplet changes after ignition. So the evolution of the droplet diameter during the whole ignition process cannot be described by a single d^2 -law. Therefore, only the vaporization rates after the ignition of the droplet are analyzed. The vaporization rates K during the combustion are determined to be 0.80 and 0.90 mm^2/s . These vaporization rates comply with the experimental results of 0.85 mm^2/s of Vieille et al. [17], and of 0.758 mm^2/s of Jackson and Avedisian [15], of 0.75 mm^2/s of Hara and Kumagai [14], and the numerical result of 0.8 mm^2/s of Cho and Dryer [29]. The ambient conditions of the studies differ considerably. For example, the ambient gas temperature is much higher in our case because the autoignition of fuel droplets in a hot gas phase is investigated. In the studies [14,15,17,29], the droplet is ignited by an ignition source. Therefore, a closer comparison of the vaporization rates is not possible. Additionally, simulations of *n*-heptane droplets vaporizing in an inert nitrogen atmosphere were performed and compared with the results of Nomura et al. [45]. In the case of a droplet placed in a nitrogen atmosphere with a temperature of 468 K and a pressure of 5 bar, we obtain a vaporization rate of 0.12 mm^2/s , compared to 0.11 mm^2/s measured by Nomura et al. [45], for a droplet with an initial diameter of 0.7 mm and at room temperature at the beginning of the simulation. Further simulations with different ambient conditions were performed, which show good agreement with the experimental results.

3.2. Flame structures and ignition locations

The detailed model makes it possible to analyze structures of the nonpremixed flame around the droplet and the detailed structures and processes during the ignition. In Fig. 2, one can see typical spatial profiles of significant species and the temperature at an early state of the ignition process. The characteristic peaks of the OH-concentration and the decrease of the *n*-heptane concentration and the oxygen concentration in the reaction zone are evident. The peaks of the OH and temperature profiles coincide and clearly identify the location of ignition and the flame

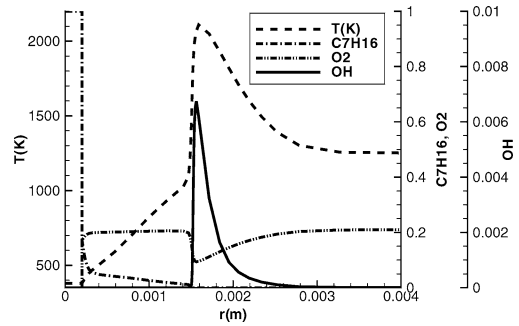


Fig. 2. Profiles of temperature and species mole fractions at an early state of ignition ($p = 7$ bar, $T_g = 1250$ K, $r_D = 200$ μm , $t = 0.67$ ms).

Table 1

Local mixtures composition at the ignition point

Ambient gas temperature T (K)	$x_{\text{NC}_7\text{H}_{16}}$	λ
800	0.0064	3.0
900	0.0084	2.3
1200	0.0085	2.3
1400	0.008	2.4
1600	0.008	2.4

front. Between droplet and reaction zone, gaseous *n*-heptane can be found, due to the vaporization of the liquid fuel and the subsequent diffusion in the gas phase. The dent of the oxygen profile indicates the oxygen consumption during the ignition process.

It is interesting to determine the composition of the mixture at the location of ignition. Table 1 shows the local mole fractions of *n*-heptane, $x_{\text{NC}_7\text{H}_{16}}$, and the resulting local air–fuel ratio.

As one can see, ignition occurs under lean conditions for all studied ambient gas temperatures, in contrast to homogeneous gas phase mixtures, which ignite faster under rich conditions. The reason is that in the case of droplet ignition both temperature and mixture composition show spatial variations. For hot environments both temperature prior to ignition and air–fuel ratio increase with increasing distance from the droplet. Because the temperature has a larger influence than the mixture composition on the ignition delay time, ignition will occur at a location where the temperature is high, even if the mixture is lean.

Additionally, the location of ignition (see above for its definition) is determined. For the description of technical sprays the impact of other droplets on the combustion process is of great interest. To evaluate this impact, it is relevant to determine the location of ignition. It is well known that the chemical reactions take place in the gas phase. The fuel is evaporated and afterward it is burnt. But the gaseous fuel does not ignite next to the surface of the droplet. In fact, the

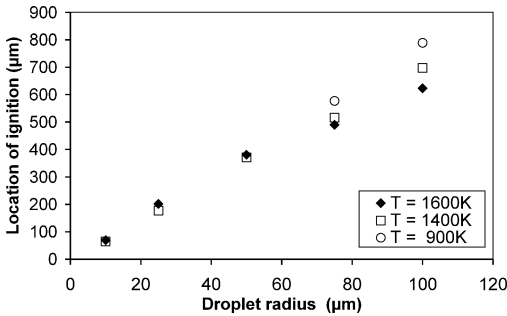


Fig. 3. Dependence of location of ignition on droplet radius ($p = 7$ bar).

investigation of the localization of the reaction zone during the ignition process showed that the location of ignition (similar to the location of the subsequent flame zone [19,30]) is a multiple of the droplet radius. In Fig. 3, one can see the proportionality of the location of ignition and the droplet radius for three different gas phase temperatures.

The ratio of the ignition radius to the droplet radius turns out to be almost constant, with a value of about 7. In the studied case, the influence of the gas temperature on the location of ignition was minor. Even for lower temperatures (900 K), the ratio of the two radii has approximately this value. Below this temperature the ratio is decreased, because two-stage ignition takes place. The first ignition stage occurs at a smaller radius, and as a result, the second ignition is located nearer to the droplet surface. Physical properties, like ambient pressure or considerably larger droplet radii, may show a significant influence on this ratio as well.

3.3. Ignition delay times

In many practical applications a knowledge of ignition delay times is very important. Examples are ignition delay times in Diesel engines or the undesired autoignition of the fuel in the premixing section of LPP gas turbines.

It is hard to control and to measure initial conditions in single-droplet experiments [34]. Especially, the initial droplet temperature and the amount of fuel in the gas phase at the start of the measurement can hardly be controlled. Therefore, simulations are performed for two different initial conditions to yield information on the sensitivity with respect to the initial conditions. On one hand, we assume no initial gaseous *n*-heptane (called INI1 in the following); on the other hand, simulations start with a small amount of pre vaporized *n*-heptane (INI2).

In this work the ignition delay time is defined as the difference in time between the exposure of the droplets to the hot environment and the ignition,

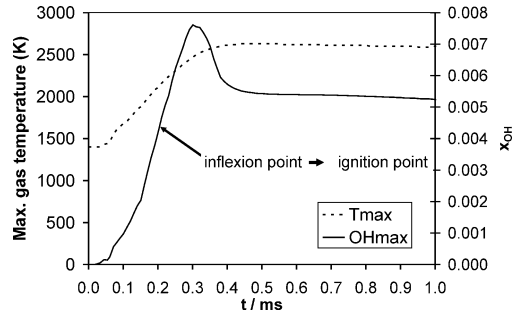


Fig. 4. Temporal evolution of maxima of spatial profiles of temperature and OH mole fraction.

characterized by the temporal evolution of the OH concentration. The ignition point is identified as the point in time with the steepest ascent of the maximum OH concentration. For this reason the maximum of the spatial OH concentration is determined for every time step. In this way the location of the flame front can be determined for every time step. The temporal evolution of the maximum OH concentration is analyzed and the inflection point is used as indicator of the steepest ascent. Fig. 4 shows the temporal evolution of the spatial maximum of the OH concentration and of the gas temperature for a simulation of an *n*-heptane droplet. The point of the time of the steepest ascent of the temperature and the OH-profile nearly coincide. This determination of the ignition point and the location of the flame front agrees with the work of Marchese et al. [16]. Furthermore, this determination of the ignition delay time is comparable to ignition delay times determined by the temperature profile, because the inflection points of the temporal profiles almost coincide. If two-stage ignition occurs at low temperatures, the first induction time is determined by the inflection point of the CH_2O -profile. In this case the inflection points of the CH_2O -profile and the temperature profile coincide.

First, the influence of the droplet temperature on the ignition delay time shall be investigated. This is of interest, because many simplified models assume constant temperature in the droplet. We calculate ignition delay times with a fixed droplet temperature and with a space- and time-dependent droplet temperature, corresponding to a spatial temperature profile in the droplet obtained from the detailed model. In Fig. 5 the ignition delay times of simulations with fixed and variable droplet temperatures are compared for different gas-phase temperatures. At an ambient pressure of 7 bar the boiling temperature of *n*-heptane is 454 K. Thus a fixed droplet temperature, close to the boiling temperature, 450 K, and a lower temperature of 379 K are chosen. For calculations with variable droplet temperature the initial droplet temperature was set to 379 K.

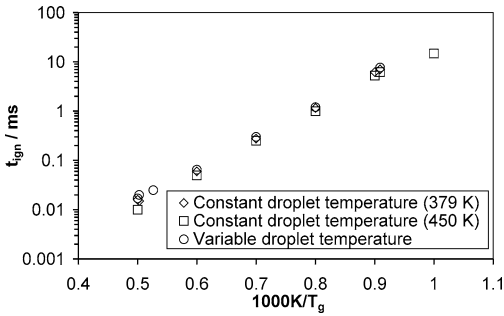


Fig. 5. Arrhenius plot of the ignition delay time for comparison of the influence of a variable and a fixed droplet temperature ($p = 7$ bar, $r_D = 100 \mu m$).

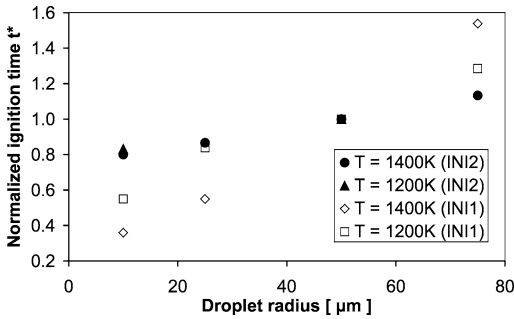


Fig. 6. Dependence of the normalized ignition delay time on the droplet radius ($p = 7$ bar).

As the plot shows, the ignition delay times of the three cases hardly differ. Thus the ignition delay time is almost independent of the droplet temperature if the initial droplet temperature is sufficiently high. However, for lower initial droplet temperatures (down to 300 K), the ignition delay time increases by a factor of about 2.

To reduce the computing time and to increase the numerical stability, further simulations are performed with a fixed droplet temperature of 379 K.

For the description of technical sprays with its droplet size distribution it is of interest to study the effect of varying droplet radii on the ignition delay time. Fig. 6 shows the ignition delay time t^* normalized on the droplet radius. The droplet radius is varied from 10 to 75 μm . The normalization is performed by dividing the ignition delay time by the ignition delay time of a droplet radius of 50 μm at the same gas phase temperature:

$$t^* = \frac{t_{ign}(r_D)}{t_{ign}(r_D = 50 \mu m)}. \quad (28)$$

As Fig. 6 shows, an increase of the droplet radius causes an increase of the ignition delay time in the studied cases. This increase depends strongly on the chosen initial conditions. If n -heptane in the gas phase

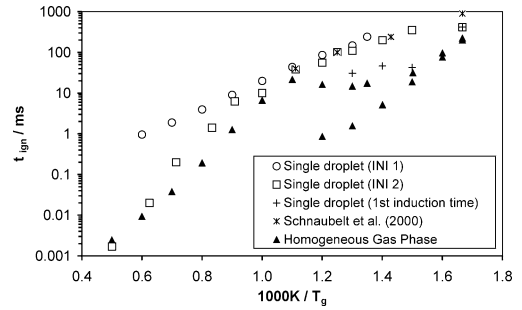


Fig. 7. Arrhenius plot of the dependence of the ignition delay time on ambient gas temperature ($p = 7$ bar, single droplets $r_D = 200 \mu m$, homogeneous gas phase $\lambda = 1$).

is assumed to be absent initially, the ignition delay time increases by a factor of about 5 for droplet radius varying from 10 to 75 μm at an ambient temperature of 1400 K. The increase of the ignition delay time with increasing droplet radius is also observed by Tsukamoto et al. [32] and Moriue et al. [37]. These studies show that this behavior depends crucially on the ambient conditions, such as pressure or overall equivalence ratio. At an ambient temperature of 1200 K, the increase of the ignition delay time with increasing droplet radius decreases to a factor of about 2.5. For an ambient temperature of 900 K, even a slight increase of ignition delay time with decreasing droplet radius is observed (not shown in Fig. 6). This slight increase is in agreement with results from the literature [31,33], where the ignition delay times of n -heptane have been shown to decrease slightly with increasing droplet diameter. Fig. 6 also shows the considerable dependence on the initial conditions at high temperatures. One can see a minor variation of the ignition delay time if initial gaseous n -heptane exists (INI2). In this case the droplet radius has a minor effect on the ignition delay times, compared to the calculations with other initial conditions (INI1).

The ambient gas-phase temperature is the physical property with the largest influence on the ignition delay time. Therefore, the dependence of the ignition delay time on the gas-phase temperature is determined for a temperature range from 600 to 2000 K with an ambient pressure of 7 bar and a droplet radius of 200 μm . Simulations of igniting droplets were performed with the two different initial conditions for the amount of n -heptane in the gas phase. In Fig. 7, the temperature dependence of ignition delay times can be seen. In the temperature range between 650 and 850 K two-stage ignition behavior is observed. Therefore, total ignition delay times and first induction times are included in Fig. 7. Additionally, the first and total ignition delay times of a homogeneous stoichiometric gaseous n -heptane/air mixture are shown.

In the Arrhenius plot (Fig. 7) one can see the typical temperature dependence of the ignition delay time of a homogeneous *n*-heptane/air mixture. The ignition delay time depends strongly on the temperature below 700 K and above 900 K. In the range between 700 and 900 K the significant decrease of the ignition delay time with decreasing temperature (NTC behavior) can be seen. In this range two-stage ignition is observed. The first and total ignition delay times are shown in the figure. This points out the validity of the mechanism for high-temperature as well as for low-temperature kinetics. Fig. 7 also shows the ignition delay times of single droplets for two different initial conditions. Above 1000 K the temperature dependence of the ignition delay time in the case of prevaporized *n*-heptane (INI2) is stronger than that in the case of no initial gaseous *n*-heptane (INI1). The single droplets with the initial condition INI2 have a shorter ignition delay time because of prevaporized *n*-heptane. In the case of no initial gaseous *n*-heptane (INI1), the physical transport processes, such as vaporization and diffusion, are rate-limiting and the contribution of the chemical kinetics to the ignition delay time plays a minor role. Below 1000 K the ignition delay times of INI1 and INI2 appear to be almost the same. The ignition delay time increases with decreasing temperature. A decrease of the ignition delay times of the droplets with decreasing temperature, which would correspond to the NTC behavior of the homogeneous gas phase, cannot be observed. The first induction time of the droplets shows nearly no temperature dependence (ZTC behavior) in the range of 650 to 760 K. In this temperature range the slope of the temperature dependence of the ignition delay time of the single droplets differs strongly from that in the homogeneous gas phase. For droplets the slope remains almost the same as in the high-temperature region (above 1000 K), whereas the behavior of the homogeneous gas phase changes dramatically at about 900 K. This points out the strong interaction between physical and chemical processes. In addition, the total ignition delay times of Schnaubelt et al. [35] are shown in Fig. 7. They show the same qualitative behavior (note, however, that these results refer to different ambient conditions, $r_D = 350 \mu\text{m}$, $p = 5 \text{ bar}$). Other experimental studies [31,33] show similar qualitative behavior, too.

In different technical applications (e.g., gas turbines, internal combustion engines) autoignition of droplets appears at different ambient pressures. Therefore, we investigate the pressure dependence of the ignition delay time. In Fig. 8 the pressure dependences of the ignition delay time of an *n*-heptane droplet with a radius of $50 \mu\text{m}$ and of the stoichiometric homogeneous *n*-heptane/air gas mixture at an

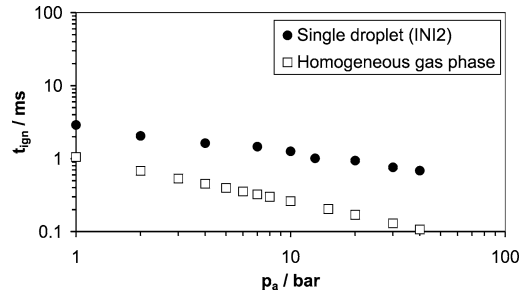


Fig. 8. Dependence of ignition delay time on ambient pressure ($T_g = 1200 \text{ K}$, single droplets $r_D = 50 \mu\text{m}$, homogeneous gas phase $\lambda = 1$).

ambient gas temperature of 1200 K are shown in the range from 1 to 40 bar.

A decrease of the ignition delay time with increasing pressure is observed. The scaling of both axes of this figure is logarithmic. Therefore the linear decrease of the ignition delay time indicates a rational dependence following the power law

$$t_{\text{ign}}(p) \propto \left(\frac{p}{p_0}\right)^{-0.4} \quad (29)$$

The decrease of the ignition delay can be explained mainly by the speedup of the chemical kinetics. On the other hand, the vaporization rate is not much affected by the increasing pressure. This fact is for example shown by Nomura et al. [45]. Despite changing the initial conditions from INI2 to INI1, almost the same behavior is observed. The results are in good agreement with Tsukamoto et al. [32] and Nakanishi et al. [33], who determined a similar decrease of the ignition delay time with increasing ambient pressure at lower temperatures. A qualitatively similar dependence of the ignition delay time can be observed in the case of the homogeneous *n*-heptane/air gas mixture. In this case the exponent of the power law is determined to approximately -0.6 .

4. Conclusions

Autoignition of single *n*-heptane droplets in air is simulated for a wide range of conditions. The simulations are performed with a detailed vaporization model, detailed transport models, and a detailed reaction mechanism.

The temporal evolution of the droplet diameter follows a d^2 -law after ignition in all studied cases. The presented vaporization rates are in good agreement with the experimental and numerical results taken from the literature. Nevertheless, a description of the temporal evolution during the whole ignition process by one single d^2 -law is not possible. Detailed

investigations showed the ignition to occur in zones of lean mixture, but of high temperature. The ratio of the radius of ignition to the droplet radius has been about 7 for ambient temperatures greater than 900 K. Below this temperature the ratio decreases. The influence of different physical parameters on the ignition delay time was investigated. At least for the conditions considered here, the dependence of the ignition delay time on the droplet temperature is insignificant. The influence of the droplet radius on the ignition delay time cannot be described by one single behavior or law. Initial conditions, as well as ambient gas temperature, have an influence on the radius dependence, not only quantitatively but qualitatively. The dependence of the ignition delay time on the droplet radius increases with increasing ambient temperature. The ambient gas temperature turns out to have the largest influence on the ignition delay time. Primarily in the high-temperature region, the temperature dependence is sensitive to the initial conditions. Compared to a homogeneous gas mixture, the behavior of a single fuel droplet is different and the slope of the Arrhenius plot is diminished. Especially, NTC behavior cannot be observed. With increasing ambient pressure the ignition delay time decreases. This decrease follows a rational law with an exponent of -0.4 . This behavior is similar to previous results obtained at different ambient conditions.

The results obtained in this study can be used to produce droplet ignition and combustion libraries for subsequent use in flamelet spray modeling. Future work will deal with the investigation of the autoignition of isooctane droplets. Further studies will be on the ignition process of multicomponent droplets, such as *n*-heptane/isooctane droplets, for a better modeling of technical fuels.

Acknowledgment

The authors thank the DFG for financial support in the frame of SFB 606.

References

- [1] H.-J. Bauer, Prog. Comput. Fluid Dynam. 4 (2004) 130–142.
- [2] V. Golovitchev, N. Nordin, R. Jarnicki, J. Chomiak, SAE Paper 2000-01-1891.
- [3] C. Law, Prog. Energy Combust. Sci. 8 (1982) 171–201.
- [4] G. Faeth, Proc. Combust. Inst. 26 (1996) 1593.
- [5] H. Chiu, Prog. Energy Combust. Sci. 26 (2000) 381–416.
- [6] C. Hollmann, E. Gutheil, Combust. Sci. Technol. 135 (1998) 175–192.
- [7] D. Spalding, Proc. Combust. Inst. 4 (1953) 847–864.
- [8] W. Sirignano, Prog. Energy Combust. Sci. 9 (1983) 291–322.
- [9] M. Burger, R. Schmehl, K. Prommersberger, O. Schäfer, R. Koch, S. Wittig, Int. J. Heat Mass Transfer 46 (2003) 4403–4412.
- [10] S. Wittig, M. Hallmann, M. Scheurlen, R. Schmehl, A new Eulerian model for turbulent evaporating sprays in recirculating flows, in: AGARD-CP-536, 1993, pp. 37.1–37.11.
- [11] F. Sparrow, J. Gregg, Trans. ASME 80 (1958) 879–886.
- [12] H. Chiu, L. Hu, Proc. Combust. Inst. 27 (1998) 1889–1896.
- [13] G. Faeth, D. Olson, SAE Trans. (1968) 1793–1802.
- [14] H. Hara, S. Kumagai, Proc. Combust. Inst. 23 (1990) 1605–1610.
- [15] G. Jackson, C. Avedisian, Proc. R. Soc. London Ser. A Math. Phys. Eng. Sci. 446 (1994) 255–276.
- [16] A. Marchese, F. Dryer, R. Colantonio, V. Nayagam, Proc. Combust. Inst. 26 (1996) 1209–1217.
- [17] B. Vieille, C. Chauveau, X. Chesneau, A. Odeide, I. Gökalp, Proc. Combust. Inst. 26 (1996) 1259–1265.
- [18] V. Nayagam, J. Haggard Jr., R. Colantonio, A. Marchese, F. Dryer, B. Zhang, F. Williams, AIAA J. 36 (1998) 1369–1378.
- [19] K. Okai, O. Moriue, M. Araki, M. Tsue, M. Kono, J. Sato, D. Dietrich, F. Williams, Combust. Flame 121 (2000) 501–512.
- [20] C. Chauveau, I. Gökalp, D. Segawa, T. Kadota, H. Enomoto, Proc. Combust. Inst. 28 (2000) 1071–1077.
- [21] B. Shaw, H. Dwyer, J. Wei, Combust. Sci. Technol. 174 (2002) 29–50.
- [22] S. Cho, M. Choi, F. Dryer, Proc. Combust. Inst. 23 (1990) 1611–1617.
- [23] S. Cho, R. Yetter, F. Dryer, J. Comput. Phys. 102 (1992) 160–179.
- [24] P. Stapf, Modellierung der Tröpfchenverbrennung unter Einschluß detaillierter chemischer Reaktion, Ph.D. thesis, Universität Stuttgart, 1992.
- [25] Y. Aouina, U. Maas, E. Gutheil, U. Riedel, J. Warnatz, Combust. Sci. Technol. 173 (2001) 1–23.
- [26] A. Kazakov, J. Conley, F. Dryer, Combust. Flame 134 (2003) 301–314.
- [27] G. Jackson, C. Avedisian, Combust. Sci. Technol. 115 (1996) 125–149.
- [28] P. Stapf, H. Dwyer, R. Maly, Proc. Combust. Inst. 27 (1998) 1857–1864.
- [29] S. Cho, F. Dryer, Combust. Theory Model. 3 (1999) 267–280.
- [30] A. Marchese, F. Dryer, V. Nayagam, Combust. Flame 116 (1999) 432–459.
- [31] M. Takei, T. Tsukamoto, T. Niioka, Combust. Flame 93 (1993) 149–156.
- [32] T. Tsukamoto, H. Okada, T. Niioka, Jpn. Soc. Aeronaut. Space Sci. Trans. 35 (1993) 165–176.
- [33] R. Nakanishi, H. Kobayashi, S. Kato, T. Niioka, Proc. Combust. Inst. 25 (1994) 447–453.
- [34] M. Tanabe, M. Kono, J. Sato, J. Koenig, C. Eigenbrod, F. Dinkelacker, H. Rath, Combust. Sci. Technol. 108 (1995) 103–119.
- [35] S. Schnaubelt, O. Moriue, T. Coordes, C. Eigenbrod, H. Rath, Proc. Combust. Inst. 28 (2000) 953–960.
- [36] S. Schnaubelt, O. Moriue, C. Eigenbrod, H. Rath, Micrograv. Sci. Technol. XIII (1) (2001) 20–23.

- [37] O. Moriue, M. Mikami, K. Kojima, C. Eigenbrod, Proc. Combust. Inst. 30 (2005) 1973–1980.
- [38] U. Maas, J. Warnatz, Proc. Combust. Inst. 22 (1988) 1695–1704.
- [39] V. Golovitchev, available at: <http://www.tfd.chalmers.se/~valeri/MECH.html>.
- [40] J. Hirschfelder, C. Curtiss, R. Bird, Molecular Theory of Gases and Liquids, Wiley, New York, 1964.
- [41] R. Reid, J. Prausnitz, B. Poling, The Properties of Gases and Liquids, fourth ed., McGraw–Hill, New York, 1989.
- [42] U. Maas, Mathematische Modellierung instationärer Verbrennungsprozesse unter verwendung detaillierter chemischer Reaktionsmechanismen, Ph.D. thesis, Universität Heidelberg, 1988.
- [43] F. Fritsch, J. Butland, SIAM J. Sci. Stat. Comput. 5 (1984) 300.
- [44] P. Deuffhard, E. Hairer, J. Zugck, Numer. Math. 51 (1987) 501–516.
- [45] H. Nomura, Y. Ujiiie, H. Rath, J. Sato, M. Kono, Proc. Combust. Inst. 26 (1996) 1267–1273.